ADVANCED MATERIALS

www.advmat.de

AFM-Based Spin-Exchange Microscopy Using Chiral Molecules

Amir Ziv, Abhijit Saha, Hen Alpern, Nir Sukenik, Lech Tomasz Baczewski, Shira Yochelis, Meital Reches, and Yossi Paltiel**

Local magnetic imaging at nanoscale resolution is desirable for basic studies of magnetic materials and for magnetic logic and memories. However, such local imaging is hard to achieve by means of standard magnetic force microscopy. Other techniques require low temperatures, high vacuum, or strict limitations on the sample conditions. A simple and robust method is presented for locally resolved magnetic imaging based on short-range spin-exchange interactions that can be scaled down to atomic resolution. The presented method requires a conventional AFM tip functionalized with a chiral molecule. In proximity to the measured magnetic sample, charge redistribution in the chiral molecule leads to a transient spin state, caused by the chiral-induced spin-selectivity effect, followed by the exchange interaction with the imaged sample. While magnetic force microscopy imaging strongly depends on a large working distance, an accurate image is achieved using the molecular tip in proximity to the sample. The chiral molecules' spin-exchange interaction is found to be 150 meV. Using the tip with the adsorbed chiral molecules, two oppositely magnetized samples are characterized, and a magnetic imaging is performed. This method is simple to perform at room temperature and does not require high-vacuum conditions.

Scanning probe microscopy (SPM) utilizes a physical sharp probe for imaging with atomic resolution. The scanning tunneling microscope[1] (STM), measures the tunneling current between a tip and a scanned surface which depends exponentially on the tip–surface distance. This fast decay of the tunneling current is a critical part in STM effective use, since it allows a very sensitive feedback loop effective for a single or few atoms at the edge of the tip. These atoms only take part in the interaction enabling atomic resolution. Other high-resolution techniques followed the STM, employing short-range interactions such as the atomic force microscope[2] (AFM) and near field scanning optical microscope[3] (NSOM).

High-resolution magnetic imaging is challenging in that sense. In magnetic force microscopy[4] (MFM), the magnetic force between a magnetized tip and a scanned surface is measured by magnetic dipole–dipole interaction which is long range (decay as r^{-3}). The magnetized area of the probe cannot be smaller than a single domain (around 30 nm in size). Therefore, the obtained signal is an integration of the magnetic dipoles of the entire tip active area with the dipoles in the sample. This limits the spatial resolution of the MFM. Furthermore, at short tip–sample distances, the magnetic interaction is weak compared to other interactions, such as the van der Waals interaction which enforces measuring at large tip–sample distance reducing the acquired resolution further.

Spin-polarized STM (SPSTM) is done by filtering one spin,[5,6] using a magnetic probe enhancing the resolved magnetic imaging. However, this method requires a conductive sample, preferably low temperatures and always ultra-high vacuum conditions. In scanning SQUID microscopy (SSM) superconducting quantum interference device (SQUID) is placed on a tip and allows magnetic imaging.[7] Although the sensitivity of SQUID is very high, this technique usually allows resolution of microns and requires cryogenic conditions. Reducing the SQUID size to the nanoscale reduces sensitivity and the resolution is few tens of nanometers.[8] Another magnetic imaging technique[9] takes advantage of the magneto-optical Kerr effect (MOKE), in general terms, the change in the angle of rotation polarization plane between the incident

A. Ziv, H. Alpern, N. Sukenik, Dr. S. Yochelis, Prof. Y. Paltiel
Applied Physics Department
The Hebrew University of Jerusalem
Jerusalem 9190401, Israel
E-mail: paltiel@mail.huji.ac.il

A. Ziv, Dr. A. Saha, H. Alpern, N. Sukenik, Dr. S. Yochelis, Prof. M. Reches, Prof. Y. Paltiel
Center for Nanoscience and Nanotechnology
The Hebrew University of Jerusalem
Jerusalem 9190401, Israel
E-mail: meital.reches@mail.huji.ac.il

Dr. A. Saha, Prof. M. Reches
Institute of Chemistry
The Hebrew University of Jerusalem
Jerusalem 9190401, Israel

Prof. L. T. Baczewski
Magnetic Heterostructures Laboratory
Institute of Physics, Polish Academy of Sciences
Al. Lotnikow 32/46, 02-668 Warszawa, Poland

The ORCID identification number(s) for the author(s) of this article can be found under https://doi.org/10.1002/adma.201904206.

DOI: 10.1002/adma.201904206

and the reflected light beam is interpreted as the magnetization influence of the studied sample. While this technique overcomes the slow decaying of the magnetic stray field, it is diffraction limited and does not allow ultra-high-resolution imaging. In recent years measuring magnetization is also done by placing a diamond with a single nitrogen vacancy (NV) defect on an AFM tip.[10–12] In that case the Zeeman splitting in the NV center is exploited for sensitive magnetic imaging. This technique allows high resolution (down to the nanoscale) at ambient conditions since the imaging is not limited by the wavelength of the fluorescence (it is not diffraction limited), but by the NV–surface distance. Nevertheless, the technique still relays on the stray magnetic field and it is not straight forward to deduce the magnetization of the scanned sample, and usually prior knowledge is required about the sample magnetic stray field,[13,14] while it is not easy to reproduce a single NV defect at the same location.

An entirely different approach for magnetic imaging is to use the spin exchange interaction as the SPM signal instead of the magnetic dipole–dipole interaction. Since the exchange interaction is purely quantum, it is short range as the overlapping between the relevant wavefunctions already vanishes at small separation distances. An SPM technique which exploits the exchange interaction for magnetic imaging is called the magnetic exchange force microscopy[15] (MExFM) allowing atomic resolution of a magnetic imaging. In MExFM, a magnetic AFM tip is operated in non-contact mode at very close distances to obtain the magnetic exchange signal. To distinguish between the magnetic exchange signal from other interactions such as electrostatic and van der Waals, it is mandatory that the magnetic moments in the sample are chemically identical. This limits the range of samples which can be measured using this technique. Moreover, it requires ultra-high vacuum, cryogenic temperatures, and high external magnetic field to align the magnetic moment of the tip. It is thus highly desired to have a simple system which relies on the magnetic spin exchange interaction without limitation on the scanned sample or measurement conditions, with a simple tip perpetration to function at ambient conditions, as presented here.

We exploit the chiral induced spin selectivity effect[16,17] (CISS) in which electron motion in a chiral molecule results in spin filtering. This electron movement can be achieved by an external voltage bias[18–20] or by charge reorganization due to a chemical bonding.[21,22] A helical (and chiral) polypeptide, alpha helix polyalanine (AHPA), is adsorbed on a gold AFM cantilever. When the molecule is in proximity to the sample, charge redistributes in the molecule due to a change in the induced dipole. This redistributed charge wavefunction becomes spin polarized by the CISS effect. When the wavefunctions of the molecule and magnetized sample overlap, the spatial hybrid wavefunction will be either symmetric or anti-symmetric to the exchange of electrons according to the alignment of the corresponding spins. This difference is manifested in a different force felt by the AFM cantilever and is the heart of this study. In principle, very few molecules participate, and the exchange interaction is short range allowing the measurement of local magnetization, with the potential of reaching atomic resolution. All the while using a functionalized tip which is easy to fabricate and functions at room temperature. The abovementioned concept is illustrated in **Figure 1**b.

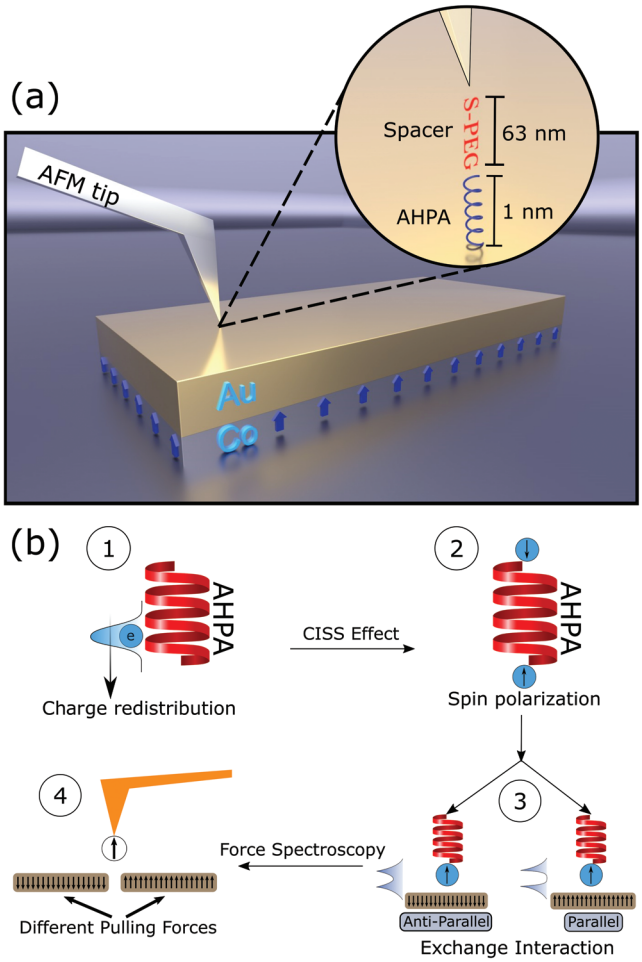

Figure 1. a) Inset: An AHPA molecule is adsorbed on an Au covered AFM tip. The molecule under study is separated from the tip by a PEG molecule to reduce electrostatic interactions between the tip and the substrate. Also, the system is immersed in ethanol to reduce capillary forces. The sample under study is the MBE grown Co-based nanostructure with out-of-plane easy axis. b) When the tip is close to the sample, reorganization of the electric charges in the molecule (1) results in spin filtering due to the CISS effect (2), which is followed by an exchange interaction between the molecular wavefunction and the wavefunction of the substrate (3), this interaction is sensed by the deflection of the AFM cantilever (4). Different interaction strength is sensed for two opposite sample magnetizations.

The experimental setup is demonstrated in Figure 1a. A standard silicon gold AFM tip covered with a gold layer is thiol bonded to a polyethylene glycol (PEG) molecule, 63 nm in length, which is bonded through an amine group to an L-AHPA molecule. The synthesis process ensured that the side of the molecule exposed to the studied sample will be that of the COOH group, so the orientation of the AHPA is constant and no covalent bonding will arise between the molecule and the surface under study. The PEG molecule serves as a spacer which reduces non-specific interactions between the Au covered tip and the sample. During the measurements the tip and the sample were immersed in ethanol to eliminate any capillary forces.

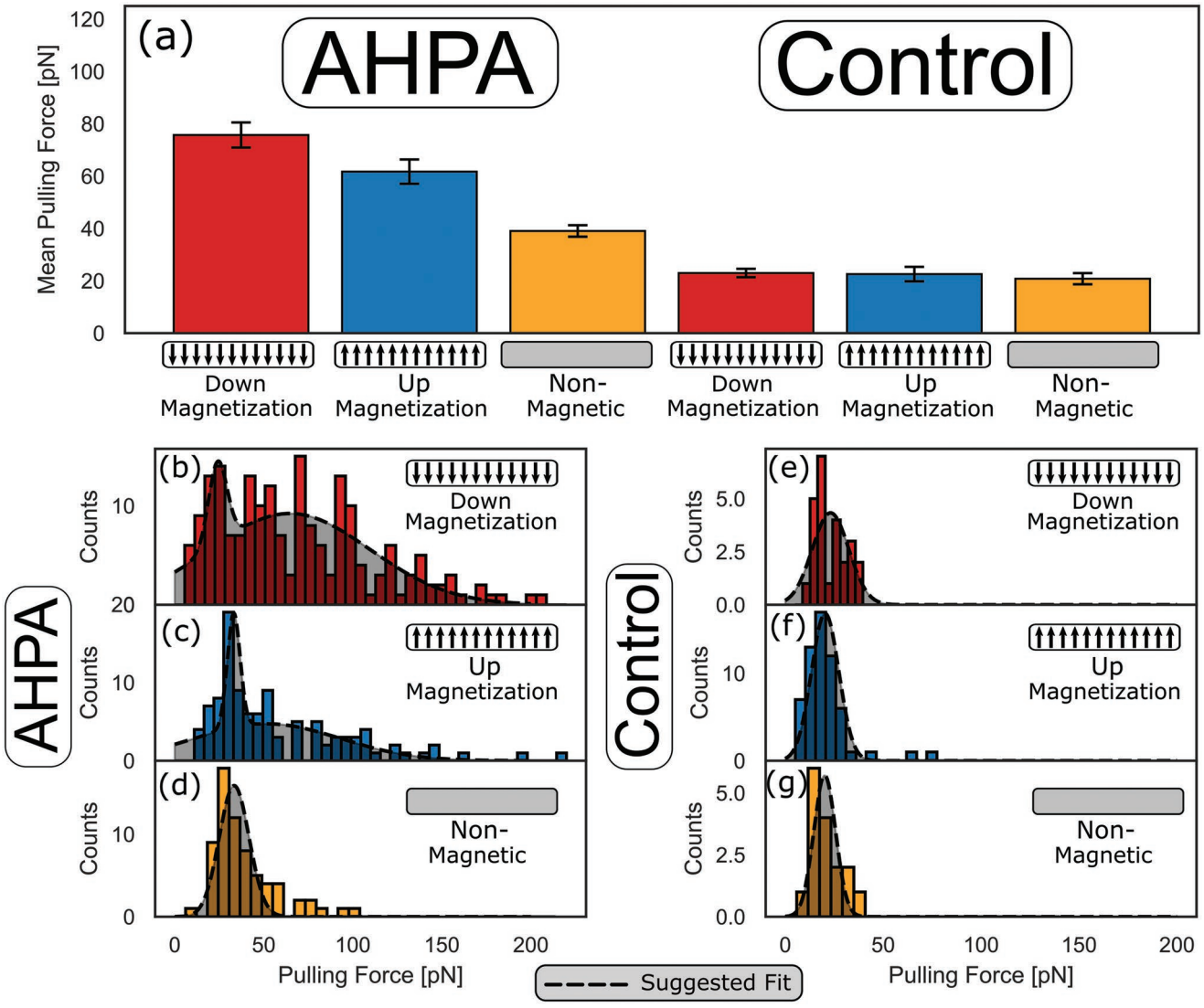

Figure 2. Force spectroscopy results. a) The mean pulling force for two molecules, AHPA and a control molecule. For the AHPA, a difference in force exists between the up and down magnetization, whereas such difference is not present for the control molecule. Also, comparing to the results for a non-magnetic sample, the exchange interaction introduces a strong pulling force in addition to the standard non-specific interactions. The presented error is the standard error of the mean. b–g) Pulling force distribution for each of the measurements. For the AHPA molecule (b, c, d) the forces distribution is wider, which can be attributed to the additional stretching of the molecule due to the additional exchange interaction. For the AHPA results a sum of two Gaussian functions is better fitted, while a single Gaussian is enough for all other measurements.

To demonstrate the differences between the symmetric and anti-symmetric states of the system, hundreds of force spectroscopy curves were taken using the same functionalized AFM tip, on the oppositely magnetized ferromagnetic samples. An atomically flat ferromagnetic surface was used, to avoid any discrepancies between the composition and topography. The sample studied was a molecular beam epitaxy (MBE) grown nanostructure of Al_2O_3/Pt/Au/Co(2 nm)/Au(5 nm) with well-defined easy axis perpendicular to the sample plane. The Au layer prevents the Co layer oxidation. A control sample of 25 nm Au deposited without cobalt was used for comparison.

About 1000 force curves were collected by the AFM for each measurement step. Each force curve was inspected separately, and only those force curves which showed pronounced pulling event were kept for further analysis, where the pulling force, the force required to pull the molecule from the sample, was calculated, in a similar way as done in previous works.[23,24] The experiment was performed with a control molecule as well, in which the helical AHPA molecule was replaced with a linear carbon chain molecule. The results are presented in **Figure 2**a, where a force difference of 13.98 ± 6.67 (pN), between up and down perpendicular magnetization direction of the Al_2O_3/Pt/Au/Co(2 nm)/Au(5 nm) sample, is evident (Figure 2a, left side). Repeating the same experiment for the same sample using the control molecule showed no difference between the two magnetization directions and a non-magnetic sample (Figure 2a, right). Since both the AHPA and the control molecules are terminated with a COOH group, the chemical affinity to the

gold interface is similar, thus we ascribe the force differences between the up and down magnetization directions to the chiral nature of the AHPA. Also, as was shown by Crespo et al., a sulfur–gold bond can induce magnetic properties in gold nanoparticles,[25] but since there is no difference in the measured force between the two magnetization directions by the control molecule, this explanation can be ruled out.

Notably, the force is weaker for the sample without a ferromagnetic layer using the AHPA molecule. Repeating the experiment with the control molecule the force remains constant for all samples and is weaker compared to the AHPA. This indicates that the exchange interaction introduces an additional force to the system. The distribution of forces in Figures 2d–g spreads up to about 50 pN, which corresponds to non-specific interactions. In Figures 2b,c, in which AHPA molecule and a magnetized substrate are used, the force spreads further as a result of the additional specific interaction which we relate to the spin exchange interaction between the AHPA and the magnetized substrate. For clarity, a fit to a sum of two Gaussian functions for the AHPA measurements (Figure 2b,c) is presented. The additional force is related to stretching of the molecule when the exchange interaction is prominent. This force is not presented for the control molecule.

Using this method, the energy of the exchange interaction can be obtained by calculating the breaking energy, integrating the force curve from the pulling position to the zero-force position sensed by the cantilever. An example of such an integral is shown in **Figure 3** (grey area). The obtained difference in energy between the up and down magnetization of 150 ± 50 (meV) (Figure 3, inset), is in agreement with first principles calculations done in an attempt to describe the molecular spin exchange energy.[18,20]

Importantly, imaging with the AHPA molecule functionalized gold AFM tip is achieved using standard force mapping technique. In this technique, a force spectroscopy curve is obtained for each pixel, and the minimum value of the curve is taken as the imaging signal. Imaging was done on a commercially available magnetic tape sample (purchased from Bruker). The sample consists of oppositely magnetized stripes covered homogenously with no correlation between the topography or surface chemistry of the sample and the magnetic stripes.

The magnetic stripes are clearly shown in the force mapping image presented in **Figure 4**a as in the image obtained by a conventional MFM given for comparison (Figure 4e). Figure 4b shows an analyzed cross section of the force curves, the maximal force is presented at the relevant distance for different points of the cross section. The maximal force of the curve is measured at a very small tip–sample distance of the order of several nanometers. This points out the importance of spin exchange interactions in addition to the magnetic dipole–dipole interaction as it is obtained at small tip–sample separation distance. The dynamics of the effect can be probed by changing the extended delay time, which is the time when the tip remains in contact with the sample surface before retraction. The dependence of the molecular electronic distribution reorganization dynamics on the spin exchange is studied by increasing the delay time from 0 to 1 s. Indeed, the contrast of the image was reduced (Figure 4c). We ascribed

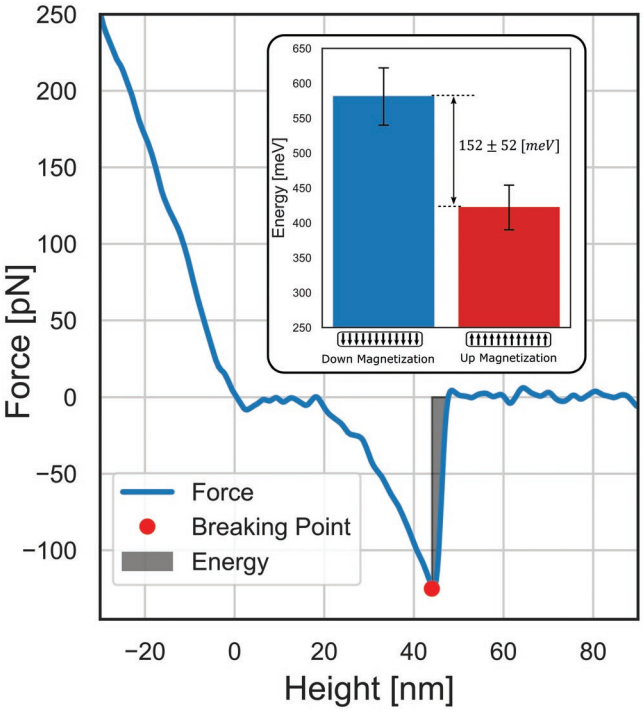

Figure 3. Typical force dependence on the tip–surface distance, the pulling point of the molecule and the integrated area represent the pulling energy of the molecule. Inset: The mean pulling energy for the up and down direction of perpendicular sample magnetization, showing a difference of 150 meV. The presented error is the standard error of the mean.

these results to T_1, the spin coherence time, in the polarized molecule. The dependence of the molecular spin exchange interaction on the duration of the reaction time was also observed in a previous study,[22] where the specific interaction of the spin with magnetized substrate was found to be very long on the order of 2 s.

Overall, the observed interactions originating from molecular/sample spin exchange are very strong and demonstrate the potential to perform local, highly resolved magnetization imaging up to the atomic scale. The results also probe the interaction energy which supply the base for enantiomer separation techniques using magnetic substrates.

To show that the suggested mechanism of spin exchange magnetic mapping is different from standard MFM it is beneficial to compare the imaging results of the magnetic tape sample. In MFM, the magnetic stray field which results from the sample is measured, while in spin exchange the magnetization of the sample is imaged directly and locally. Thus, to deduce the magnetization pattern of the sample in the MFM, some prior knowledge of the sample is required to deduce the magnetization from the stray field. In Figure 4d,e, MFM images for the magnetic tape are presented for different tip–sample distances. It is evident that the stripes are getting wider with increasing tip–sample distance (see Figure S1, Supporting Information for all the intermediate tip–sample distances). In magnetostatics, when no electrical current or change in time of the magnetic field exists, it is common to calculate the magnetic stray field using electrostatics, assigning "magnetic charges" to

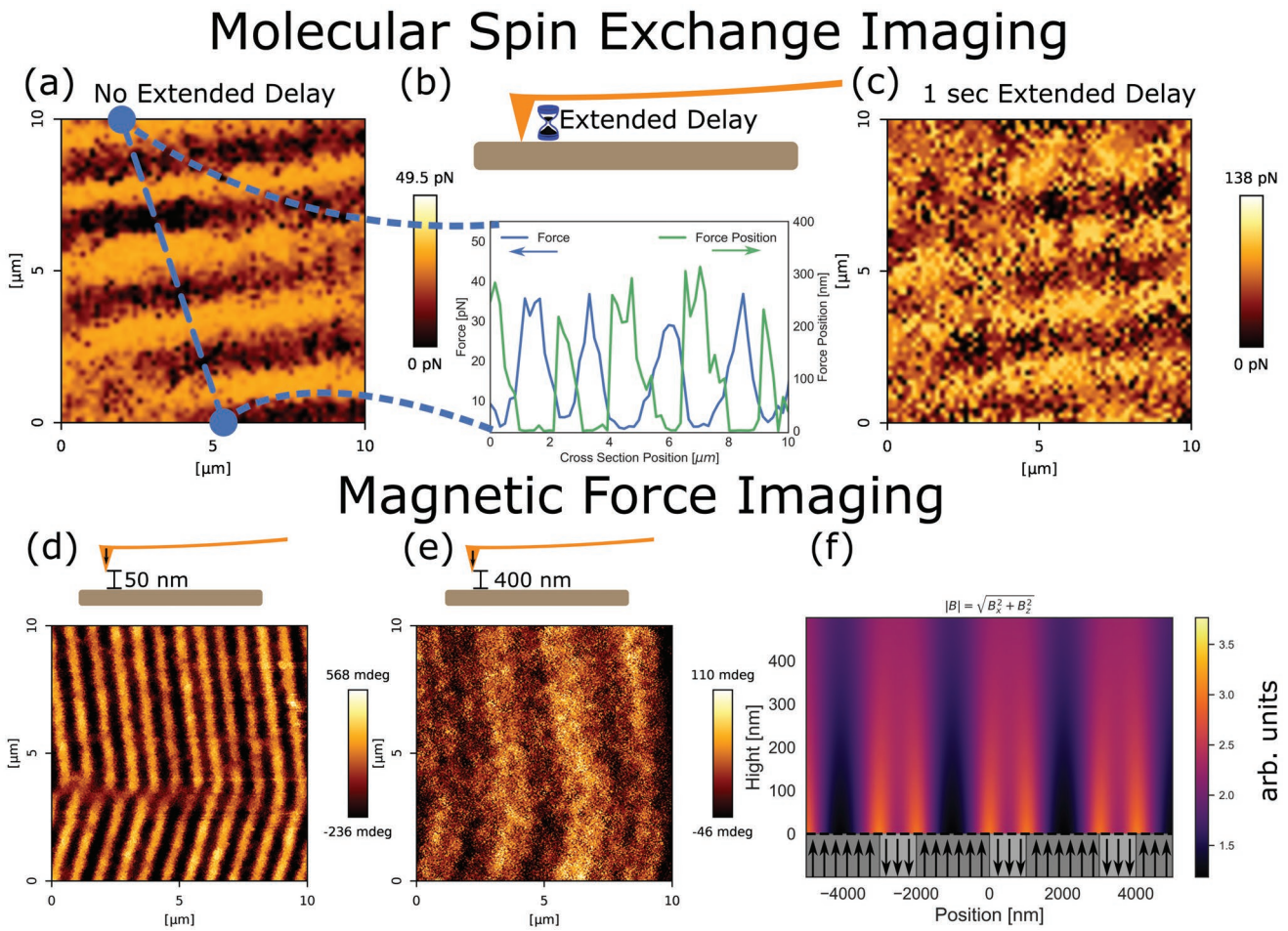

Figure 4. a) Molecular spin exchange force mapping of a magnetic tape sample. Stripes are clearly shown. b) Top—the "extended delay time" is the duration of the time when the tip remains in contact with a sample surface before retracting. Bottom—cross section of the force mapping image, showing that the maximal force is measured at a very close proximity to the surface, suitable for exchange interaction. c) Force mapping image at 0 extended delay, showing a reduction in the contrast. d) MFM image, of the same magnetic tape sample, obtained at a tip–sample distance of 50 nm. e) MFM image, obtained at a tip–sample distance of 400 nm. f) Magnetic stray field magnitude calculation for the magnetic tape sample, relaying on the data obtained from the molecular spin exchange image. As the tip–sample distance is increased (the *y* axis) the stripes are widened.

the sample. Therefore, the magnetic sample with the out–of-plane (OOP) magnetization can be analyzed in the same way as a parallel plate capacitor (see Supporting Information for more details). Hence, for a large area of magnetization compared to the tip distance the magnetic field can be measured only at the edges of the stripe.[13,14] This explains the widening of the stripes observed at different tip–sample heights. In Figure 4g, a calculation of the magnetic stray field magnitude is shown as a function of the tip–sample distance (*Y* axis) for magnetic stripe with OOP up magnetization of 2 μm width, separated by 1 μm stripes with down magnetization, which corresponds roughly to the experimental results shown in Figure 4a. As the tip–sample distance is increased, the individual stripes get wider and are merging. Therefore, we can deduce the same image obtained by MFM using a prior knowledge already acquired from the CISS AFM image.

In summary, we report here an efficient and easy microscopy method to perform local magnetic imaging based on spin exchange interaction at room temperature with a standard gold-coated AFM tip functionalized with a chiral molecule. The preparation of the tip is straightforward and does not require advanced lithography techniques or applying an external magnetic field. The presented CISS AFM method has the potential for a robust way to image magnetization at a very high resolution, in principle up to atomic resolution, with easy interpretation of the magnetic image. We believe that the simplicity and generality of this method, alongside with the use of the spin exchange interaction instead of magnetic field detection, opens an opportunity to achieve magnetic imaging of any magnetic sample with very high resolution. Lastly, this concept allows measuring the spin exchange interactions of chiral molecules and magnetic samples reaching large energies of 150 meV at short range as predicted by theory.[20] This quantitative measurement is highly important for local scanning of magnetic materials, and for obtaining full control of enantiomer separation methods based on the interaction of chiral molecules with magnetic substrates.[22]

Experimental Section

Molecules Synthesis: The thiol functionalized PEGylated chiral (and helical) polypeptide, AHPA [HS-PEG-NH-AAAAKAAAAKAAAAKAAAAK AAAAKAAAAKAAAAK-COOH], and the thiol functionalized PEGylated control molecule [HS-PEG-NH-6-Ahx-K-COOH] were synthesized on solid phase following solid phase peptide synthesis procedure using microwave peptide synthesizer (CEM, Discover Bio). The lysine residue in the control molecule has a weak CISS effect and thus has little influence on the observed phenomena. Fmoc-L-Lys (Boc)-Wang resin (0.343 meq gm^{-1} and 100–200 mesh) was used as solid support. The resin was swelled overnight in dichloromethane (DCM) and *N*,*N*′-dimethyl formamide (DMF) solvent mixture (1:1) prior to the synthesis. The Fmoc deprotection was performed by 20% piperidine in DMF and coupling reaction was performed using Oxyma pure and *N*,*N*′-diisopropylcarbodiimide (DIC) in DMF solvent under microwave. Fmoc-L-Ala-OH, Fmoc-L-Lys (Boc)-OH, and NHS-PEG-S-Trt (purchased from Iris Biotech GmbH, Germany) were used to make the chiral AHAP. Fmoc-6-Ahx-OH (purchased from Sigma-Aldrich Inc., Israel) and NHS-PEG-S-Trt were used to make the control compound. Ninhydrin test was performed at each step of coupling and Fmoc deprotection to check whether the reaction was completed or not. The resin was washed five times with each of the following solvents DMF, DCM, methanol, and diethyl ether and kept under vacuum for 4 h to ensure complete dryness. Cleavage cocktail containing 92.5% TFA, 2.5% TIPS, 2.5% EDT, and 2.5% water was used. The molecule attached on the resin was taken with the cocktail mixture and shacked for 4 h at room temperature. The solution was drained and poured into ice cold diethyl ether for precipitation. It was kept at –20 °C for overnight and centrifuged at 5000 rpm at 4 °C. The residue was taken, dissolved it in water, and lyophilized. A white solid compound was obtained.

Tip Functionalization: The solid compound was dissolved in triple distilled water to prepare 1 mM solution. The Au-coated tip was washed with EtOH, dried in air, and incubated with the 1 mM solution of the molecule overnight at room temperature. The tip was again washed with water to remove the non-attached molecules and dried in air.

Magnetic Sample Preparation: The ferromagnetic thin films used in the experiments were a sandwich Au/Co/Au type epitaxial nanostructures of Al_2O_3(0001)/Pt/Au/Co (thickness 1.5–2.2 nm)/Au (thickness 5 nm) with the easy magnetization axis in the OOP direction. Thin films were deposited in the MBE Prevac system with the base pressure of 10^{-11} Torr. Epitaxial growth mode was confirmed by RHEED observations. Different Co layer thicknesses were deposited, resulting in different coercive field values. Hysteresis loops for all the studied samples with different Co thicknesses were measured in situ by using polar MOKE proving the perpendicular anisotropy in each sample.

Force Spectroscopy Measurements: Force spectroscopy curves were obtained using JPK AFM (*NanoWizard3*). A commercial gold-coated tip (Bruker OBL-10) was functionalized by immersing the tip for 20 min in ethanol and then by overnight adsorption of the abovementioned molecules. 1000 force curves were obtained for each molecule and each sample. The loading rate for the AHPA molecule was 8.198 and 31.475 nN s^{-1} for the control molecule. Then only curves which showed a pronounced pulling event were kept, where a wormlike chain model was fitting to the curves after smoothing and calibration of the curves. The magnetic samples were magnetized in a determined direction prior to the measurements by applying 3T magnetic field.

Force Mapping Imaging: A 64 × 64 pixel image was obtained by acquiring a force curve for each pixel. The minimum value was used to contrast the image. Nearest neighbor averaging and a low pass filter were used for clarity. The imaged sample was a commercially available magnetic tape purchased from Bruker.

MFM Measurement: Magnetic force imaging was done using JPK AFM (*NanoWizard3*) at hover mode for magnetic imaging. MikroMasch HQ:NSC36/CO-CR/AL BS probe was used. The imaging was done for tip–sample distance between 50 and 400 nm at 50 nm jumps.

Supporting Information

Supporting Information is available from the Wiley Online Library or from the author.

Acknowledgements

A.Z. and A.S. contributed equally to this work. Y.P. acknowledges the support from the Volkswagen Foundation (No. VW 88 367), the Israel Science Foundation (ISF Grant No. 1248/10), and John Templeton foundation (60796). A.Z. would like to acknowledge the Israeli Ministry of Science, Technology and Space support. A.S. acknowledges the support of the Shunbrun Fellowship, Hebrew University of Jerusalem.

Conflict of Interest

The authors declare no conflict of interest.

Keywords

atomic force microscopy, chiral molecules, magnetic imaging, spin exchange

Received: July 2, 2019
Revised: August 6, 2019
Published online: August 18, 2019

[1] G. Binnig, H. Rohrer, *Rev. Mod. Phys.* **1987**, *59*, 615.
[2] G. Binnig, C. F. Quate, Ch. Gerber, *Phys. Rev. Lett.* **1986**, *56*, 930.
[3] E. Betzig, A. Lewis, A. Harootunian, M. Isaacson, E. Kratschmer, *Biophys. J.* **1986**, *49*, 269.
[4] Y. Martin, H. K. Wickramasinghe, *Appl. Phys. Lett.* **1987**, *50*, 1455.
[5] R. Wiesendanger, H.-J. Güntherodt, G. Güntherodt, R. J. Gambino, R. Ruf, *Phys. Rev. Lett.* **1990**, *65*, 247.
[6] M. Bode, *Rep. Prog. Phys.* **2003**, *66*, 523.
[7] R. C. Black, A. Mathai, F. C. Wellstood, E. Dantsker, A. H. Miklich, D. T. Nemeth, J. J. Kingston, J. Clarke, *Appl. Phys. Lett.* **1993**, *62*, 2128.
[8] D. Vasyukov, Y. Anahory, L. Embon, D. Halbertal, J. Cuppens, L. Neeman, A. Finkler, Y. Segev, Y. Myasoedov, M. L. Rappaport, M. E. Huber, E. Zeldov, *Nat. Nanotechnol.* **2013**, *8*, 639.
[9] P. Kasiraj, R. Shelby, J. Best, D. Horne, *IEEE Trans. Magn.* **1986**, *22*, 837.
[10] J. M. Taylor, P. Cappellaro, L. Childress, L. Jiang, D. Budker, P. R. Hemmer, A. Yacoby, R. Walsworth, M. D. Lukin, *Nat. Phys.* **2008**, *4*, 810.
[11] G. Balasubramanian, I. Y. Chan, R. Kolesov, M. Al-Hmoud, J. Tisler, C. Shin, C. Kim, A. Wojcik, P. R. Hemmer, A. Krueger, T. Hanke, A. Leitenstorfer, R. Bratschitsch, F. Jelezko, J. Wrachtrup, *Nature* **2008**, *455*, 648.
[12] L. Rondin, J.-P. Tetienne, P. Spinicelli, C. Dal Savio, K. Karrai, G. Dantelle, A. Thiaville, S. Rohart, J.-F. Roch, V. Jacques, *Appl. Phys. Lett.* **2012**, *100*, 153118.
[13] T. Hingant, J.-P. Tetienne, L. J. Martínez, K. Garcia, D. Ravelosona, J.-F. Roch, V. Jacques, *Phys. Rev. Appl.* **2015**, *4*, 014003.
[14] J.-P. Tetienne, T. Hingant, L. J. Martínez, S. Rohart, A. Thiaville, L. H. Diez, K. Garcia, J.-P. Adam, J.-V. Kim, J.-F. Roch, I. M. Miron, G. Gaudin, L. Vila, B. Ocker, D. Ravelosona, V. Jacques, *Nat. Commun.* **2015**, *6*, 6733.

[15] U. Kaiser, A. Schwarz, R. Wiesendanger, *Nature* **2007**, *446*, 522.
[16] K. Ray, S. P. Ananthavel, D. H. Waldeck, R. Naaman, *Science* **1999**, *283*, 814.
[17] R. Naaman, Y. Paltiel, D. H. Waldeck, *Nat. Rev. Chem.* **2019**, *3*, 250.
[18] O. B. Dor, S. Yochelis, S. P. Mathew, R. Naaman, Y. Paltiel, *Nat. Commun.* **2013**, *4*, 2256.
[19] G. Koplovitz, D. Primc, O. B. Dor, S. Yochelis, D. Rotem, D. Porath, Y. Paltiel, *Adv. Mater.* **2017**, *29*, 1606748.
[20] A. Kumar, E. Capua, M. K. Kesharwani, J. M. L. Martin, E. Sitbon, D. H. Waldeck, R. Naaman, *Proc. Natl. Acad. Sci. U. S. A.* **2017**, *114*, 2474.
[21] O. Ben Dor, S. Yochelis, A. Radko, K. Vankayala, E. Capua, A. Capua, S.-H. Yang, L. T. Baczewski, S. S. P. Parkin, R. Naaman, Y. Paltiel, *Nat. Commun.* **2017**, *8*, 14567.
[22] K. Banerjee-Ghosh, O. B. Dor, F. Tassinari, E. Capua, S. Yochelis, A. Capua, S.-H. Yang, S. S. P. Parkin, S. Sarkar, L. Kronik, L. T. Baczewski, R. Naaman, Y. Paltiel, *Science* **2018**, *360*, 1331.
[23] Y. Razvag, V. Gutkin, M. Reches, *Langmuir* **2013**, *29*, 10102.
[24] P. Das, T. Duanias-Assaf, M. Reches, *J. Vis. Exp.* **2017**, *121*, 54975.
[25] P. Crespo, R. Litrán, T. C. Rojas, M. Multigner, J. M. de la Fuente, J. C. Sánchez-López, M. A. García, A. Hernando, S. Penadés, A. Fernández, *Phys. Rev. Lett.* **2004**, *93*, 087204.